



## Deceleration efficiencies of shrub windbreaks in a wind tunnel



Xiaoxu Wu<sup>a,b</sup>, Xueyong Zou<sup>b,\*</sup>, Na Zhou<sup>b</sup>, Chunlai Zhang<sup>b</sup>, Sha Shi<sup>c</sup>

<sup>a</sup> College of Global Change and Earth System Science, Beijing Normal University, Beijing 100875, PR China

<sup>b</sup> State Key Laboratory of Earth Surface Processes and Resource Ecology, Beijing Normal University, Beijing 100875, PR China

<sup>c</sup> College of Life and Environment Sciences, Central University for Nationalities, Beijing 100081, PR China

### ARTICLE INFO

#### Article history:

Received 20 March 2014

Revised 14 September 2014

Accepted 7 October 2014

#### Keywords:

Shrub windbreaks

Airflow field

Deceleration efficiency

Wind velocity gradient

### ABSTRACT

Artemisia and Salix are dominant shrub species for windbreaks in arid areas of China, and they show similar features to shrubs in other arid areas of the world. We compared the mean velocity fields and shelter effects of two shrub windbreaks with different layouts. For a single plant of Artemisia, the higher the free airflow velocity is, the more the wind velocity around two sides of the plant increases. The velocity gradient around a single plant of Salix is smaller than that around an Artemisia plant due to the difference in the plant shapes. Seven new velocity zones in the horizontal direction appear when airflow passes through an Artemisia windbreak, including four deceleration zones and three acceleration zones. The mean velocity field that is affected by a Salix windbreak can be divided into a deceleration zone in the front, an acceleration zone above, a vortex zone behind and a restoration zone downwind of the vortex zone. Shelter effects of the shrub windbreaks vary with the wind velocity and are influenced by the construct of the windbreaks. Shrub windbreaks that have a complex construction have better shelter effects than simple ones. The shelter effects of plant windbreaks are also influenced by the growth features of the plants. Considering the plant characteristics and the shelter effects of Salix and Artemisia windbreaks, it is optimal to plant these two windbreaks together in a sand-control system. This research is intended to be useful for sand movement control in arid areas.

© 2014 Elsevier B.V. All rights reserved.

### 1. Introduction

China is one of the most severely desertified countries in the world, with up to 3.3 million km<sup>2</sup> desertified lands (Decai, 1998; Zhong and Qu, 2003). Recently, desertification has become a major environmental problem and has attracted widespread attention in China, especially in the arid, semi-arid and dry semi-humid climatic zones. The desertification process is generally accompanied by soil and vegetation degradation, water and wind erosion (Dregen, 1998). In China, 50% of the desertified lands lies in the agro-pastoral transition zone of northern China (Zhao and Masayuki, 1997; Zhu and Cheng, 1994). This desertified transition region serves as the main source of sand that was carried aloft by windstorms and ultimately distributed throughout the country's eastern regions as heavy layers of dust (Zhang and Shi, 2003). The Mu Us Sandland located in the agro-pastoral transition zone is typical sandland in semi-arid China in terms of its vegetation,

its high frequency of blown-sand disasters and its sand-control counter-measures.

Shrubs have been observed to be an important biological measure to control desertification and soil erosion (Li et al., 2013), and usually shrubs that live locally are considered to be the best materials to cover and stabilize the sand because they are effective, persistent and low-cost (Yang et al., 2006). In areas where water availability limits the plant coverage, desert shrubs might form fertility islands (an accumulation of resources around individual plants) (Perroni-Ventura et al., 2006; González-Ruiz et al., 2007). Furthermore, local shrubs, in the long run, can enforce the stability of deposition (Burylo et al., 2011, 2012a). Therefore, local shrubs are effective at both controlling sand movement in desert areas and reducing soil erosion in farmlands. The local vegetation in the Mu Us Sandland is composed chiefly of shrubs in sandland, and its canopy coverage is usually especially low (Li, 1990; Zhang, 1994). The previous report indicated that the original vegetation in this sandland is mainly dominated by *Artemisia ordosica*, which is a low-growing shrub species (Wu and Yang, 2013). Therefore, we surveyed wild fields to search local vegetation species in the Mu Us Sandland. The survey revealed that *Artemisia sphaerocephala* and *Salix psammophila* are the dominant species in the Mu Us sandlands. In addition, both species have a

\* Corresponding author at: State Key Laboratory of Earth Surface Processes and Resource Ecology, Beijing Normal University, Xijiekouwai Street No. 19, Beijing 100875, PR China. Tel.: +86 010 62207162.

E-mail address: [zouxy@bnu.edu.cn](mailto:zouxy@bnu.edu.cn) (X. Zou).

high percentage of survival, grow well and are effective in reducing sand storms (Shi, 2009). *Artemisia* and *Salix* are easily available, inexpensive materials for windbreaks in the sandlands. Furthermore, both shrubs have similar dimensional characteristics to those of other shrubs in other semi-arid and arid areas, to reduce desertification and soil erosion. For example, *Hedysarum fruticosum*, *Artemisia halodendron* and *Caragana microphylla* have been planted as sand binders on moving and semi-moving sand dunes since the 1980s in the Horqin Sandy Land, which is located in the northeastern part of China (Zhang et al., 2013); Mediterranean legume shrubs, including *Colutea arborescens*, *Dorycnium pentaphyllum* and *Medicago strasser*, have been used to control soil erosion in Guadalajara in Central Spain (Garcia-Estringana et al., 2013). *Aloe secundiflora* shrubs act as facilitators in degraded semi-arid rangelands in Kenya (King, 2008). Thus, based on wind-tunnel simulations, we measured airflow field and calculated the shelter effect of these two shrub windbreaks. Scientific understanding of effective windbreaks could aid sand movement control there and can provide experience for similar arid areas in the world.

Previous researches on windbreaks are abundant. A windbreak is generally defined as any structure that reduces the wind speed (Rosenberg, 1974), and windbreaks are frequently natural vegetative barriers against wind. A windbreak can be a single element or a system of elements that, through their presence in the airflow, reduce the effects of the wind both in the immediate vicinity and within a given windward and leeward distance (Cornelis and Gabriels, 2005). The efficiency of a windbreak in terms of the reduction in the wind velocity and turbulence intensity and, hence, its efficacy on wind-erosion processes is determined by various factors (Cornelis and Gabriels, 2005). The shape, height, orientation, width and spacing all affect the wind-velocity reduction and turbulence intensity in the leeward areas of a windbreak. The free wind velocity and surface roughness of the surrounding area also affect the windbreak performance (Chepil and Woodruff, 1963; Hagen and Skidmore, 1971; FAO, 1978; Banzhaf et al., 1992). Calculating the “correct” characteristics of any specific shelter device would allow us to suggest an appropriate windbreak for any given application (Perera, 1981). Therefore, the objective of our scaled wind tunnel measurements is to design windbreaks that efficiently reduce the wind velocity and involve two shrubs (*Artemisia* and *Salix*). We compared the mean velocity fields and shelter effects of the different windbreak designs.

## 2. Simulation conditions

### 2.1. Wind tunnel measurements

The experiment was carried out in a straight-blowing wind tunnel at the State Key Laboratory of Earth Surface Processes and Resource Ecology. The test section of the wind tunnel is 24 m long, 3 m wide and 2 m high. The wind velocity could be controlled continuously from 2 to 45 m s<sup>-1</sup> and was measured using a multipoint anemometer (Wu et al., 2011). Its supporting system has a hook to connect with a three-dimensional positioning machine, by which the anemometer is transferred between the measurement points along the X, Y and Z axes (Wu et al., 2013). In this study, only the horizontal wind velocities were measured at heights of 1 cm, 3 cm, 5 cm, 7 cm, 10 cm, 15 cm, 20 cm, 25 cm, 30 cm, 40 cm, 50 cm and 60 cm. The wind velocity refers to the mean wind velocity of 120 values within 2 min. A wind tunnel simulation of the airflow around a windbreak is shown in Fig. 1.

Three types of windbreak were made: single plant, single-row and double-row. Measurement lines were set parallel to the incoming airflow, and measurement locations were placed from

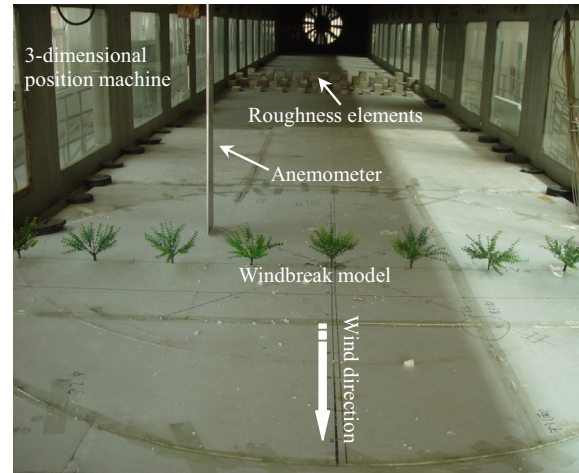


Fig. 1. Wind tunnel simulation of airflow around a single-row *Artemisia* windbreak.

upwind to downwind, with the middle of the models as the origin, point 0. The position and measurement locations for the *Artemisia* and *Salix* windbreaks in the wind tunnel are shown in Fig. 2. For the single plant *Artemisia* and *Salix* windbreaks, we measured the wind velocities in eight directions around the windbreaks, including perpendicular directions, as shown in Fig. 2A and D.

### 2.2. Wind tunnel similarity

In this experiment, we measured the pure airflow around the models; therefore, geometric similarity, movement similarity and dynamic similarity are expected to be present (Wu et al., 2003) and have the same scale. The experiment conditions in this study are roughly in line with those in the previous research (Wu et al., 2013), except for some minimal differences. Elastic parameters (because of the bending and vibration of the plants) have not been accounted for in the study.

Geometric similarity here refers to the dimensional similarity between the models in the wind tunnel and the vegetative wind barriers in the field (Wu et al., 2013). We defined the cap as the diameter length and width of the canopy of a single plant; the “row and cluster” space refers to the distance between two adjacent rows and two adjacent plants in the same row, and “the number of clusters” refers to the number of plants per row. According to our field survey, the average dimensions for the *Artemisia* branches are 80 cm in height, with a 115 cm × 117 cm cap and 160 cm × 180 cm row and cluster space, whereas for *Salix*, the average dimensions are 220 cm in height, with a 160 cm × 170 cm cap and 180 cm × 350 cm row and cluster space. Their difference lies in that (1) the architecture for a cluster of *Artemisia* is similar to a reversed cone, while for a cluster of *Salix*, it is similar to a reversed pyramid; (2) the branches of *Artemisia* are rigid, while those of *Salix* are supple. We therefore chose plastic and elastic materials with a wider coverage of width and stiff twigs, which are similar to the field *Artemisia* plants, to make the *Artemisia* windbreak models. They were made at a scale of 1:5 and were 16 cm in height, with a 23 cm × 23.5 cm cap and 32 cm × 36 cm row and cluster space. We chose tall and thin dried plant materials with soft branches, which are similar to the field *Salix* plant, to make the *Salix* windbreak models. The *Salix* windbreak models were made at a scale of 1:10 and were 22 cm in height, with a 16 cm × 17 cm cap and 18 cm × 35 cm row and cluster space (Table 1). Thus, the requirements for geometric similarity are met in this study.

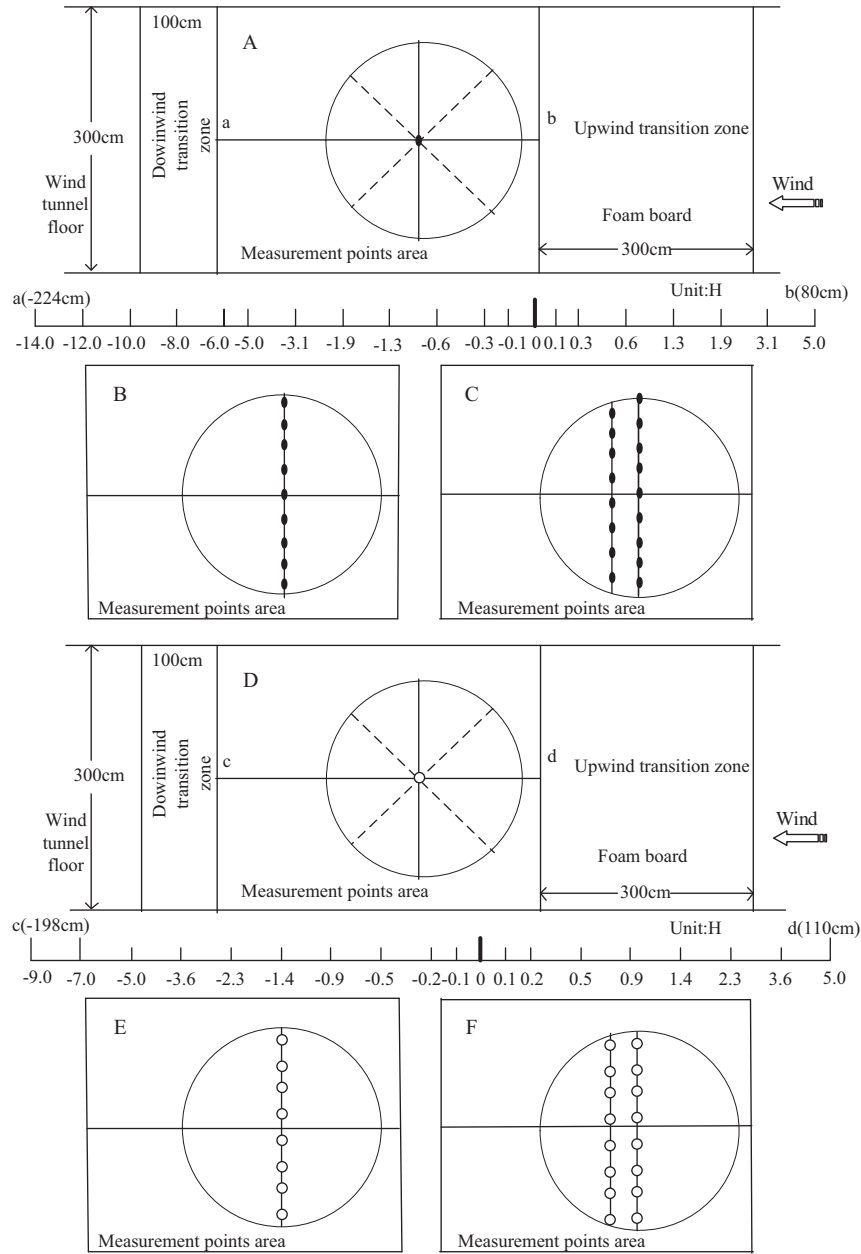


**Fig. 2.** Position and layout of measurement locations for Artemisia and Salix windbreaks in the wind tunnel. (A) Single-plant Artemisia windbreak; (B) single-row Artemisia windbreak; (C) double-row Artemisia windbreak; (D) single-plant Salix windbreak; (E) single-row Salix windbreak; (F) double-row Salix windbreak.

Movement similarity here refers to the fact that the movement route for the airflow, which corresponds to two objects with geometrical similarity, shows geometrical similarity, and the time ratio of the corresponding particle passing the corresponding distance is a constant (Wu et al., 2013). Similarly, we placed cuboid bricks as roughness elements to increase the surface friction, which can greatly reduce the inflow wind velocity and, at the same time, avoid having vortices that approach the windbreak model (Fig. 3). Movement similarity includes similarity in both the velocity and acceleration. However, the measurement of acceleration cannot be realized in a wind tunnel. Therefore, velocity similarity is used as the criterion of movement similarity, and it is determined by the wind profile power law using the following equations (Wu et al., 2013):

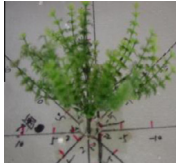



$$\frac{V_{3m}}{V_{10m}} = 0.3^{\alpha_f}, \frac{V_{18cm}}{V_{60cm}} = 0.3^{\alpha_m}, \alpha_f = \alpha_m \quad (1)$$

where  $V_{3m}$  is the wind velocity at the height of 3 m from the field measurement;  $V_{10m}$  is the wind velocity at the height of 10 m in the field, which is derived from the above measurement;  $V_{18m}$  and  $V_{60m}$  is the wind velocity, respectively, at the height of 18 cm and 60 cm in the wind tunnel;  $\alpha_f$  refers to  $\alpha$  in the field; and  $\alpha_m$  refers to  $\alpha$  in the wind tunnel.

In our study, we calculated  $\alpha_f = \alpha_m = 0.1253$ . This value is similar to the value that was used in a previous study, in which the wind profile index  $\alpha$  of a desert was determined to be 0.12 (He et al., 2006).

Statistics over accumulated time, i.e., the total number of hours from 1990 to 2005, for wind velocities that exceed the sand-blowing velocity (the critical velocity for sand movement) in the Mu Us Sandland showed that 81.68% of the wind velocity values at the height of 10 m (which corresponds to the velocity at the height of 60 cm in the wind tunnel) are 6.4–9.3 m s<sup>-1</sup>, 89.27% are 6.4–

**Table 1**  
Comparison of field real plants and wind-tunnel models.

Wind-tunnel model					Field plant	
Plant	Material	Scale	Height/cm	Morphology	Height/cm	Morphology
Artemisia	Plastic material	1:5	16		80	
Salix	Dried plant material	1:10	22		220	

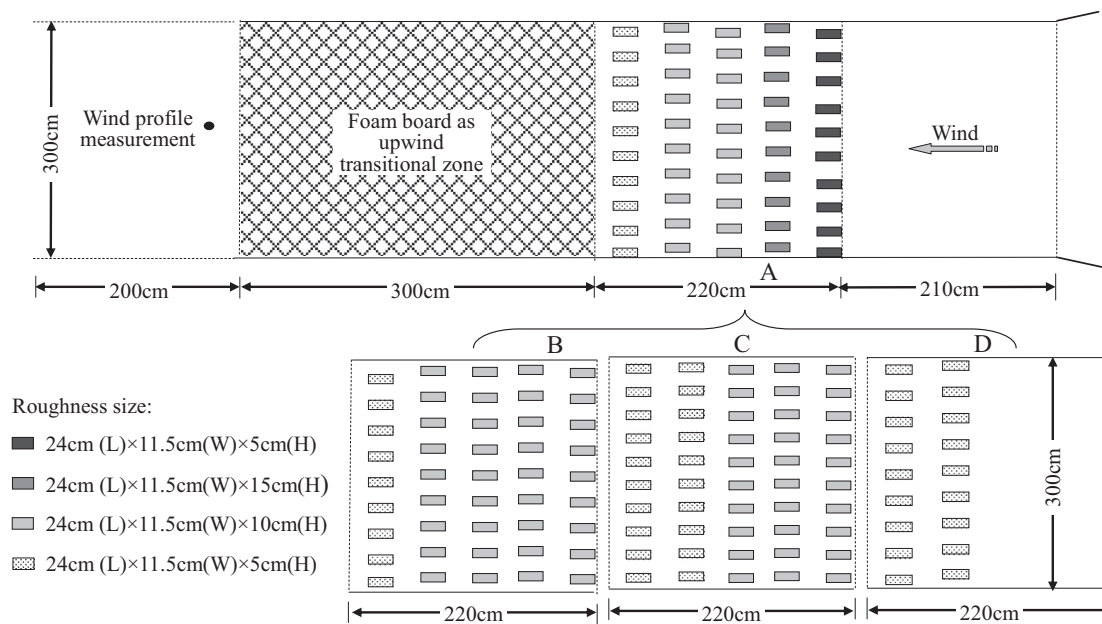


**Fig. 3.** Layout of cuboid bricks as roughness elements under different wind velocities. (A)  $5 \text{ m s}^{-1}$ ; (B)  $7.5 \text{ m s}^{-1}$ ; (C)  $10 \text{ m s}^{-1}$ ; (D)  $12.5 \text{ m s}^{-1}$ .

$10.3 \text{ m s}^{-1}$  and 98.25% are  $6.4\text{--}13.3 \text{ m s}^{-1}$  (Wu and Zou, 2011). Therefore, the experimental wind velocities that are used in this study (the wind velocity at the height of 60 cm) are  $5 \text{ m s}^{-1}$ ,  $7.5 \text{ m s}^{-1}$ ,  $10 \text{ m s}^{-1}$  and  $12.5 \text{ m s}^{-1}$ . Fig. 3 shows how the number of layers of cuboid bricks (the roughness elements) changes with the changing wind velocity. The roughness elements are paved 2.2 m-long parallel to the airflow direction.

The dynamic similarity means that the stresses for the positions of the two objects, with both geometrical similarity and movement similarity, are in proportion (Wu et al., 2013). The dynamic similarity includes the similarity in all of the forces. However, it is very difficult to measure all of the forces in a wind tunnel. Therefore, we calculated the Reynolds number (Re) as a criterion to determine the dynamic similarity in the wind-tunnel measurement, using the equation as follows (Wu et al., 2013):

$$\text{Re} = \frac{\rho V L}{\mu} \quad (2)$$

where  $\rho$  denotes the air density;  $V$  the mean air velocity;  $L$  the characteristic linear dimension; and  $\mu$  the dynamic viscosity of the air. The calculated Re is  $4.59 \times 10^5\text{--}1.91 \times 10^6$ ; thus, this measurement met the requirement for similarity in fluid dynamics (Qu et al., 2001; Wu et al., 2013).

### 3. Results

#### 3.1. The mean velocity field around the windbreaks

##### 3.1.1. The mean velocity field around the Artemisia windbreaks

The mean velocity fields around the single plant, single-row and double-row Artemisia windbreaks are shown in Fig. 4. Among them, Fig. 4A shows the velocity field around the single plant Artemisia windbreak at different heights and under different wind velocities; Fig. 4B, C and D show the velocity fields in the horizontal direction at different wind velocities, respectively, around the single plant, single-row and double-row Artemisia windbreaks.

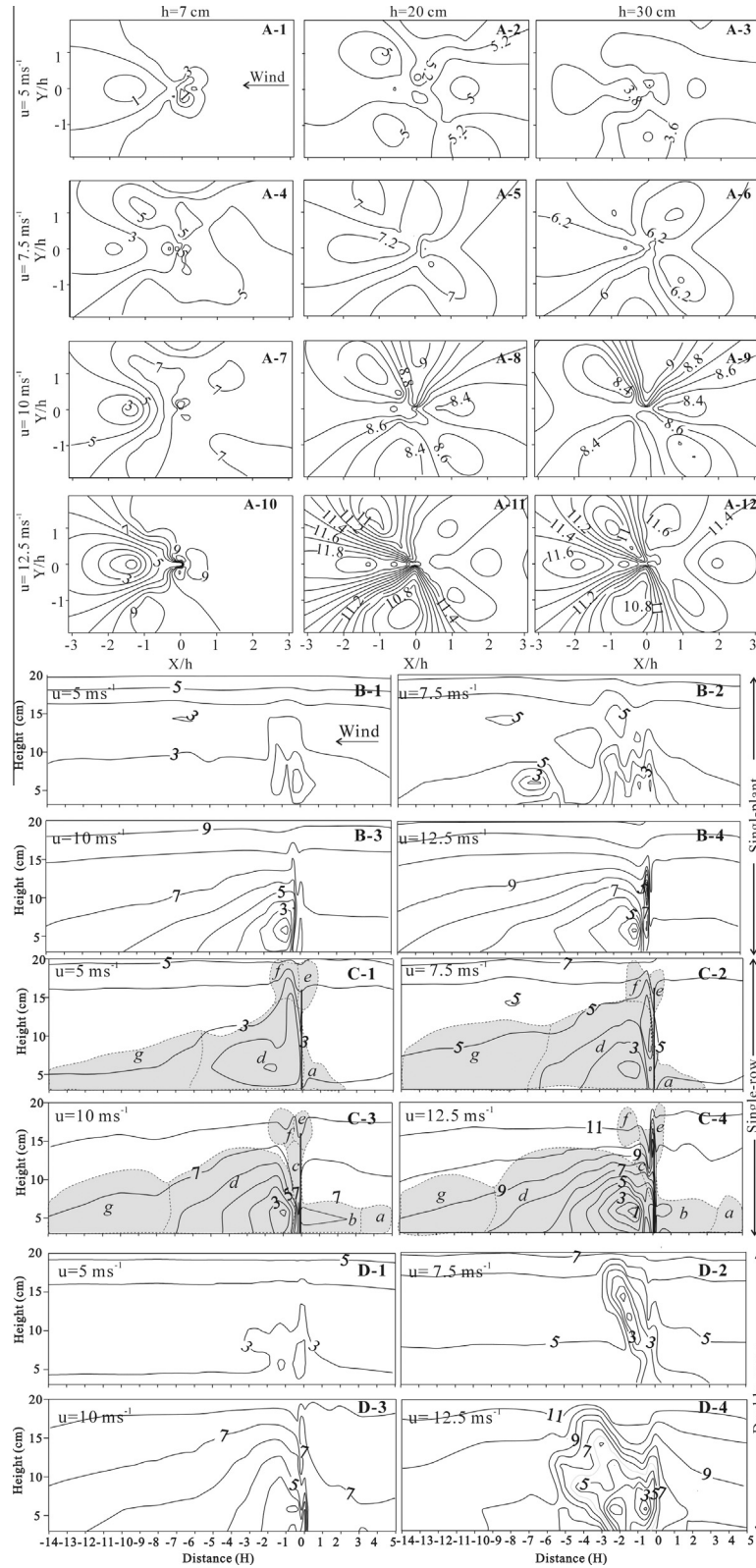


**Fig. 4.** Airflow field around different types of Artemisia windbreaks at different wind velocities. (A) Airflow field around a single-plant Artemisia windbreak in different directions; A-1,  $u = 5 \text{ m s}^{-1}$ ,  $h = 7 \text{ cm}$ ; A-2,  $u = 5 \text{ m s}^{-1}$ ,  $h = 20 \text{ cm}$ ; A-3,  $u = 5 \text{ m s}^{-1}$ ,  $h = 30 \text{ cm}$ ; A-4,  $u = 7.5 \text{ m s}^{-1}$ ,  $h = 7 \text{ cm}$ ; A-5,  $u = 7.5 \text{ m s}^{-1}$ ,  $h = 20 \text{ cm}$ ; A-6,  $u = 7.5 \text{ m s}^{-1}$ ,  $h = 30 \text{ cm}$ ; A-7,  $u = 10 \text{ m s}^{-1}$ ,  $h = 7 \text{ cm}$ ; A-8,  $u = 10 \text{ m s}^{-1}$ ,  $h = 20 \text{ cm}$ ; A-9,  $u = 10 \text{ m s}^{-1}$ ,  $h = 30 \text{ cm}$ ; A-10,  $u = 12.5 \text{ m s}^{-1}$ ,  $h = 7 \text{ cm}$ ; A-11,  $u = 12.5 \text{ m s}^{-1}$ ,  $h = 20 \text{ cm}$ ; A-12,  $u = 12.5 \text{ m s}^{-1}$ ,  $h = 30 \text{ cm}$ ; (B) airflow field around a single-plant Artemisia windbreak in horizontal direction; B-1,  $u = 5 \text{ m s}^{-1}$ ; B-2,  $u = 7.5 \text{ m s}^{-1}$ ; B-3,  $u = 10 \text{ m s}^{-1}$ ; B-4,  $u = 12.5 \text{ m s}^{-1}$ ; (C) airflow field around a single-row Artemisia windbreak in horizontal direction; C-1,  $u = 5 \text{ m s}^{-1}$ ; C-2,  $u = 7.5 \text{ m s}^{-1}$ ; C-3,  $u = 10 \text{ m s}^{-1}$ ; C-4,  $u = 12.5 \text{ m s}^{-1}$ ; a: the hindering deceleration zone upwind of the windbreak; b: the vortex deceleration zone in front of the windbreak; c: the acceleration zone within the windbreak the airflow; d: the vortex zone behind the windbreak; e: acceleration zone above the windbreak, upwind of the break; f: the acceleration zone above the windbreak, behind the windbreak; g: the airflow restoration zone. (D) airflow field around a double-row Artemisia windbreak in horizontal direction; D-1,  $u = 5 \text{ m s}^{-1}$ ; D-2,  $u = 7.5 \text{ m s}^{-1}$ ; D-3,  $u = 10 \text{ m s}^{-1}$ ; D-4,  $u = 12.5 \text{ m s}^{-1}$ .



As shown in Fig. 4A, the airflow field around the single plant *Artemisia* windbreak shows the following features. The wind velocity decreases in the leeward areas of the windbreak. At the same height, the wind velocity at the leeward side of the windbreak is lower than that at the windward; as the inflow wind velocity increases, the wind velocity increases more around the two side areas of the plant, and it has low values in the leeward areas.

As shown in Fig. 4B, C and D, the area of zero velocity expands as the wind velocity increases. For the single-row *Artemisia* windbreak, when the wind velocity is below  $12.5 \text{ m s}^{-1}$ , there is essentially no zero-velocity area within the single-row windbreak, whereas when the wind velocity is  $12.5 \text{ m s}^{-1}$ , the zero-velocity area exists leeward of the windbreak up to the distance of the height of the windbreak (0–2 cm) leeward of the windbreak. The vortex area (Fig. 4C) behind the windbreak expands as the wind velocity increases. Usually, the larger the vortex area, the slower the wind velocity recovers. The restoration of the wind velocity, which is affected by several different dimensional vortices, varies behind the windbreak at the different wind velocities and creates different downwind shelter distances. When the wind velocity is  $12.5 \text{ m s}^{-1}$ , the wind velocity is strongly reduced and quickly restored, thereby creating a shorter effective shelter distance. When the wind velocity is  $5 \text{ m s}^{-1}$ , the wind velocity is more slowly restored and creates a longer effective shelter distance.

At the same inflow wind velocity, the velocity field behaves with both similarities and differences, as shown in Fig. 4B, C and D. We will describe the situation at the wind velocity of  $10 \text{ m s}^{-1}$  in detail.

Similarly, the mean velocity field is divided into seven velocity zones, which have different aerodynamic behaviors. From upwind to downwind, they include four deceleration zones and three acceleration zones (Fig. 4C). A hindering deceleration zone is formed upwind of the windbreaks (Fig. 4C.a) because the airflow is blocked when meeting the windbreaks; this result agrees well with previous research (Judd et al., 1996). A vortex deceleration (the deceleration resulting from a vortex) zone (Fig. 4C.b) is formed in front of (just upwind of) the windbreak, and an acceleration zone (Fig. 4C.c) is formed within the windbreak due to funneling. The wind velocity is reduced again behind (just downwind of) the windbreaks, where another deceleration zone is formed (Fig. 4C.d). The wind velocity loss increases in the deceleration zone, where wind-blowing sand could be blocked and slowed down in the field. However, two acceleration zones are formed above the windbreaks, one in front of (Fig. 4C.e) and one behind the windbreaks (Fig. 4C.f). Both of them cover a limited range. The airflow restoration zone (Fig. 4C.g) exists in the area that is just above the windbreak. In the field, blowing sand within a windbreak is easily eroded, which might be the main reason for little sand deposition to occur there (Dong et al., 2007).

For the different *Artemisia* windbreaks, even though the number of velocity zones is the same, the acceleration zones within the windbreaks behave differently. Within a single plant, single-row and double-row windbreaks, the wind velocity at the height of 3 cm is, respectively, 94%, 93% and 32% of the inflow velocity. It is obvious that the wind velocity within the windbreaks decreases as the number of clusters and rows increases. The mean velocity field changes that are caused by the *Artemisia* windbreaks shows that the deceleration zones, in front, within and behind the windbreaks, can have the effect of immobilizing sand in the field (Dong et al., 2007). In the field, the acceleration within a windbreak can cause wind erosion and form a concave topology (Dong et al., 2007). Furthermore, the wind velocity at a downwind distance of 14 times the height of the model windbreak ( $x = 14 H$ ) has not been restored to the inflow wind velocity, which means that the shelter distance is longer than  $14 H$  downwind of the windbreaks. In the

field, many *Artemisia* windbreaks are built together with some space or a distance shorter than  $14 H$ , and the airflow can undergo another cycle of acceleration and deceleration before the full restoration of the wind velocity. In this way, an *Artemisia* windbreak system can effectively control the movement of blowing sand and serve as a highly efficient shelter from the wind (Dong et al., 2007).

### 3.1.2. The mean velocity field around the *Salix* windbreaks

The mean velocity fields around the single plant, single-row and double-row *Salix* windbreaks are shown in Fig. 5. Fig. 5A shows the velocity field around the single plant *Salix* windbreak at different heights and under different wind velocities; Fig. 5B, C and D show the velocity fields in the horizontal direction at different wind velocities, respectively, around the single plant, single-row and double-row *Salix* windbreaks.

As shown in Fig. 5A, under different incoming wind velocities and at different heights, the airflow field around a single plant *Salix* windbreak changes similar to that of the single plant *Artemisia* windbreak, as shown in Fig. 5A. However, the velocity isolines around the single plant *Salix* windbreak are relatively sparse compared with those around the single plant *Artemisia* windbreak. This phenomenon is caused by the difference in the two plants' shape characteristics. *Salix* is a type of typical shrub whose branches are not as dense as *Artemisia*'s, and there is little difference in the upper canopy and stem canopy, as shown in Table 1. Although the velocity isolines around the single plant *Salix* windbreak are sparse, the shelter distance of the single plant *Salix* windbreak is not necessarily smaller than that of the single plant *Artemisia* windbreak. We will discuss these aspects in detail later.

The mean velocity field in the horizontal direction is shown in Fig. 5B, C and D. Here we take the single-row *Salix* windbreak as an example. As the wind velocity increases, the wind velocity contours become denser, the airflow acceleration becomes stronger, and the area of the vortex zone behind the windbreaks increases. As the vortex area increases, the restoration of the wind velocity decreases and, thereby, increasing shelter distances are created. When the wind velocity is  $5 \text{ m s}^{-1}$ , the restoration of the wind velocity is slower, and the windbreak has a longer shelter distance. When the wind velocity is  $12.5 \text{ m s}^{-1}$ , the wind velocity behind the windbreak is strongly reduced, and the restoration of the wind velocity is more rapid, which creates a shorter shelter distance.

At the same inflow wind velocity, the velocity field behaves with both similarities and differences, as shown in Fig. 5B, C and D. Take the wind velocity of  $10 \text{ m s}^{-1}$  as an example.

Similarly, the mean velocity fields near the surface around the single plant, single-row and double-row *Salix* windbreaks could be divided into four velocity zones, which are the airflow acceleration zone upwind of the windbreaks (Fig. 5C.a), the airflow acceleration zone above the windbreaks (Fig. 5C.b), the vortex zone behind the windbreaks (Fig. 5C.c) and the airflow restoration zone downwind of the windbreaks (Fig. 5C.d). Although the mean velocity field is similarly influenced by the single plant and single-row *Salix* windbreaks, the location and range that are covered by each velocity zone for these two *Salix* windbreaks are quite different from those for the double-row *Salix* windbreak. The double-row windbreak has a larger range for the deceleration zone upwind of the windbreak than does the other two windbreaks. Therefore, the wind velocity is reduced more by the double-row windbreak than by the other two *Salix* windbreaks. In addition, the airflow acceleration zone in the area above the double-row windbreak is different from the other two windbreaks. When the airflow passes over a windbreak, the airflow direction experiences a transition from upward to horizontal to downward because the vibration of the soft herbaceous vegetation in the wind, especially the upper parts of the vegetation, reduces the accumulation of velocity in

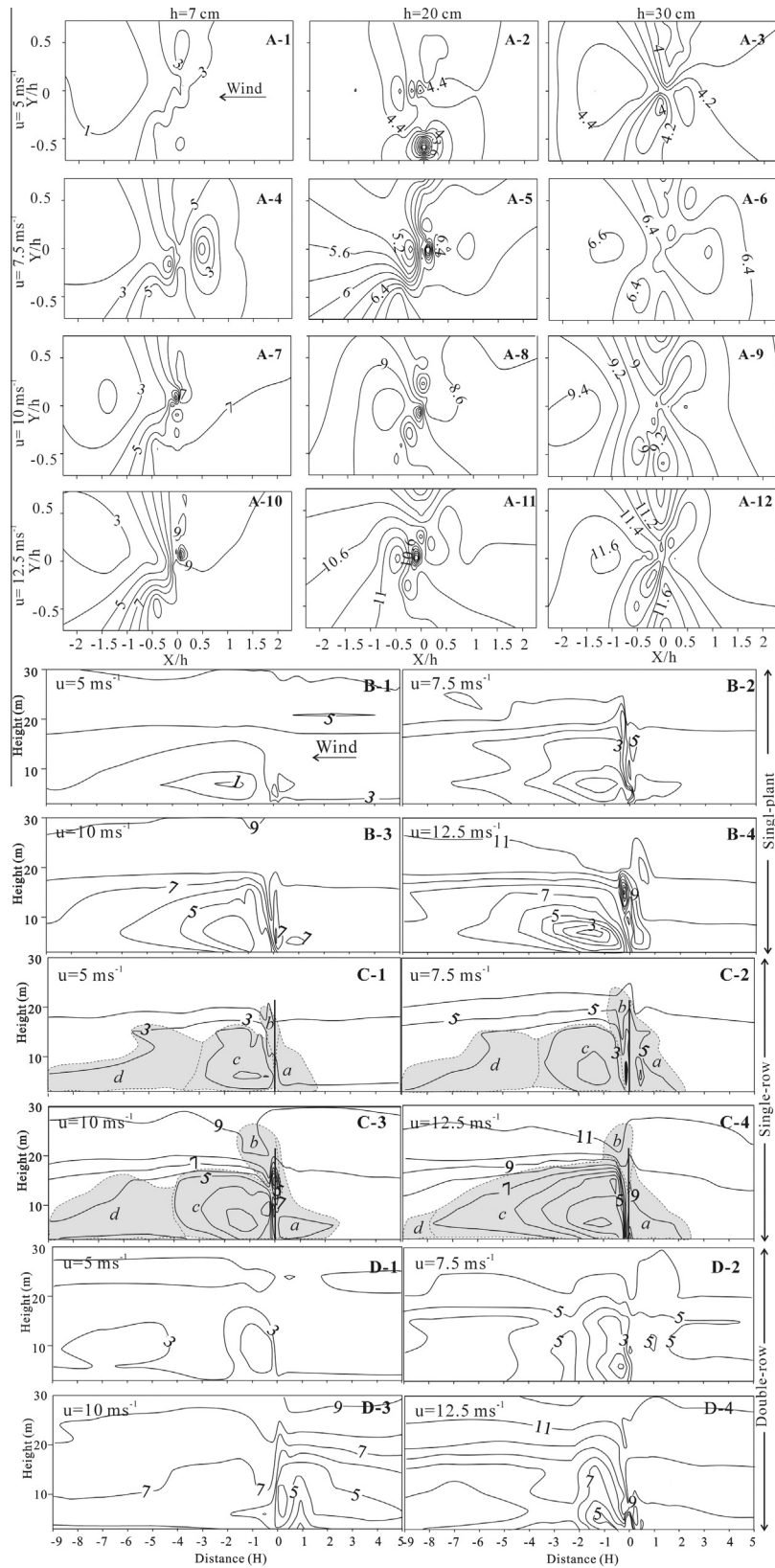


**Fig. 5.** Airflow field around different types of *Salix* windbreaks at different wind speeds. (A) Airflow field around a single-plant *Salix* windbreak in different directions; A-1,  $u = 5 \text{ m s}^{-1}$ ,  $h = 7 \text{ cm}$ ; A-2,  $u = 5 \text{ m s}^{-1}$ ,  $h = 20 \text{ cm}$ ; A-3,  $u = 5 \text{ m s}^{-1}$ ,  $h = 30 \text{ cm}$ ; A-4,  $u = 7.5 \text{ m s}^{-1}$ ,  $h = 7 \text{ cm}$ ; A-5,  $u = 7.5 \text{ m s}^{-1}$ ,  $h = 20 \text{ cm}$ ; A-6,  $u = 7.5 \text{ m s}^{-1}$ ,  $h = 30 \text{ cm}$ ; A-7,  $u = 10 \text{ m s}^{-1}$ ,  $h = 7 \text{ cm}$ ; A-8,  $u = 10 \text{ m s}^{-1}$ ,  $h = 20 \text{ cm}$ ; A-9,  $u = 10 \text{ m s}^{-1}$ ,  $h = 30 \text{ cm}$ ; A-10,  $u = 12.5 \text{ m s}^{-1}$ ,  $h = 7 \text{ cm}$ ; A-11,  $u = 12.5 \text{ m s}^{-1}$ ,  $h = 20 \text{ cm}$ ; A-12,  $u = 12.5 \text{ m s}^{-1}$ ,  $h = 30 \text{ cm}$ ; (B) airflow field around a single-plant *Salix* windbreak in horizontal direction; B-1,  $u = 5 \text{ m s}^{-1}$ ; B-2,  $u = 7.5 \text{ m s}^{-1}$ ; B-3,  $u = 10 \text{ m s}^{-1}$ ; B-4,  $u = 12.5 \text{ m s}^{-1}$ ; (C) airflow field around a single-row *Salix* windbreak in horizontal direction; C-1,  $u = 5 \text{ m s}^{-1}$ ; C-2,  $u = 7.5 \text{ m s}^{-1}$ ; C-3,  $u = 10 \text{ m s}^{-1}$ ; C-4,  $u = 12.5 \text{ m s}^{-1}$ ; a: the airflow deceleration zone upwind of the windbreak; b: the airflow acceleration zone above the windbreak; c: the vortex zone behind the windbreak; d: the airflow restoration zone downwind of the windbreaks. (D) airflow field around a double-row *Salix* windbreak in horizontal direction; D-1,  $u = 5 \text{ m s}^{-1}$ ; D-2,  $u = 7.5 \text{ m s}^{-1}$ ; D-3,  $u = 10 \text{ m s}^{-1}$ ; D-4,  $u = 12.5 \text{ m s}^{-1}$ .

the acceleration zone above the windbreak. Therefore, more Salix clusters in the double-row windbreak weaken the acceleration effect in this velocity zone. Finally, there is a much smaller vortex zone behind the double-row windbreak, where the wind velocity is restored relatively slowly. Thus, the wind velocity restoration zone downwind of the double-row Salix windbreaks has a larger range than the other two windbreaks. Therefore, the double-row Salix windbreak has a larger downwind shelter distance than the other two windbreaks.

### 3.2. The shelter effect

The shelter effect of a windbreak in reducing the wind velocity is evaluated by a dimensionless reduction coefficient  $R_{c(\Delta x, z)}$  (Cornelis and Gabriels, 2005), as follows:

$$R_{c(\Delta x, z)} = 1 - \frac{u_{\Delta x, z}}{u_{0\Delta x, z}} \quad (3)$$

where  $\Delta x$  is the distance from the windbreak (in barrier heights  $H$ );  $z$  is the height above the surface (m);  $R_{c(\Delta x, z)}$  is the wind speed reduction coefficient at the height  $z$  and the distance  $\Delta x$ ;  $u_{\Delta x, z}$  is the time-averaged wind speed that is disturbed by the windbreak ( $\text{m s}^{-1}$ ); and  $u_{0\Delta x, z}$  is the time-averaged wind speed in the absence of a windbreak ( $\text{m s}^{-1}$ ). In general, as  $R_{c(\Delta x, z)}$  increases, the shelter effect of the windbreak increases. In this study, we used  $x$  instead of  $\Delta x$ , and similarly, we used  $u_{x, z}$ ,  $u_{0x, z}$  and  $R_{c(x, z)}$  respectively instead of  $u_{\Delta x, z}$ ,  $u_{0\Delta x, z}$  and  $R_{c(\Delta x, z)}$ .

#### 3.2.1. The shelter effect of Artemisia windbreaks

##### (1) The horizontal shelter effect

To compare the horizontal shelter effect of the single plant, single-row and double-row Artemisia windbreaks, we calculated the wind velocity reduction coefficient at the height of 10 cm ( $R_{c(x, 0.1)}$ ), as shown in Fig. 6. In general,  $R_{c(x, 0.1)}$  for each measurement position is above 0 except within the windbreaks, which demonstrates that the windbreaks obviously reduce the wind velocity. For different windbreaks,  $R_{c(x, 0.1)}$  changes as the wind

velocity increases. When the wind velocity is  $5 \text{ m s}^{-1}$ , the single plant Artemisia windbreak has the largest shelter effect, both upwind and downwind. When the wind velocity is  $7.5 \text{ m s}^{-1}$ , the single plant Artemisia windbreak has the largest upwind shelter effect, and the single-row Artemisia windbreak has the largest downwind shelter effect. When the wind velocity is  $10 \text{ m s}^{-1}$ , the double-row Artemisia windbreak has the largest shelter effect both upwind and downwind. Clearly, for the double-row Artemisia windbreak,  $R_{c(x, 0.1)}$  increases as the wind velocity increases, which indicates an increasing shelter effect. We can use these data to recommend the most appropriate Artemisia windbreaks for the local prevailing wind velocity.

##### (2) The vertical shelter effect

To compare the extent of the vertical wind velocity reduction for the single plant, single-row and double-row Artemisia windbreaks, we calculated the wind velocity reduction coefficient  $R_{c(x, z)}$  at the heights of 7 cm, 20 cm and 30 cm, which, respectively, correspond to below, equal to and above the height of the windbreak. The values of  $R_{c(x, z)}$  at the wind velocity of  $10 \text{ m s}^{-1}$  are shown in Fig. 7.

Above the three windbreaks, at a height of 20 cm,  $R_{c(x, 0.2)}$  is generally negative, as shown in Fig. 7B. However, at the height of 7 cm and 30 cm,  $R_{c(x, 0.07)}$  and  $R_{c(x, 0.3)}$  are positive. This situation occurs because the flow that approaches the windbreak decelerates above the canopy but accelerates within the canopy (Judd et al., 1996). Furthermore, the acceleration is the most obvious for the single plant Artemisia windbreak, with the average  $R_{c(x, 0.2)}$  reaching  $-0.13$ . The average  $R_{c(x, 0.2)}$  for the single-row Artemisia windbreak is  $-0.03$ , and for the double-row windbreak, it is  $-0.01$ . These changes correspond with the mean velocity field change in Fig. 4C, in which the acceleration increases as the mean velocity field changes more rapidly.

In the area below the windbreak height,  $R_{c(x, 0.07)}$  varies, as shown in Fig. 7A. For the single plant Artemisia windbreak,  $R_{c(x, 0.07)}$  is the greatest from upwind  $5H$ – $3.1H$ . For that same height,  $R_{c(x, 0.07)}$  for the double-row Artemisia windbreak is the greatest from upwind  $1.9H$  to downwind  $-0.1H$ , whereas it is

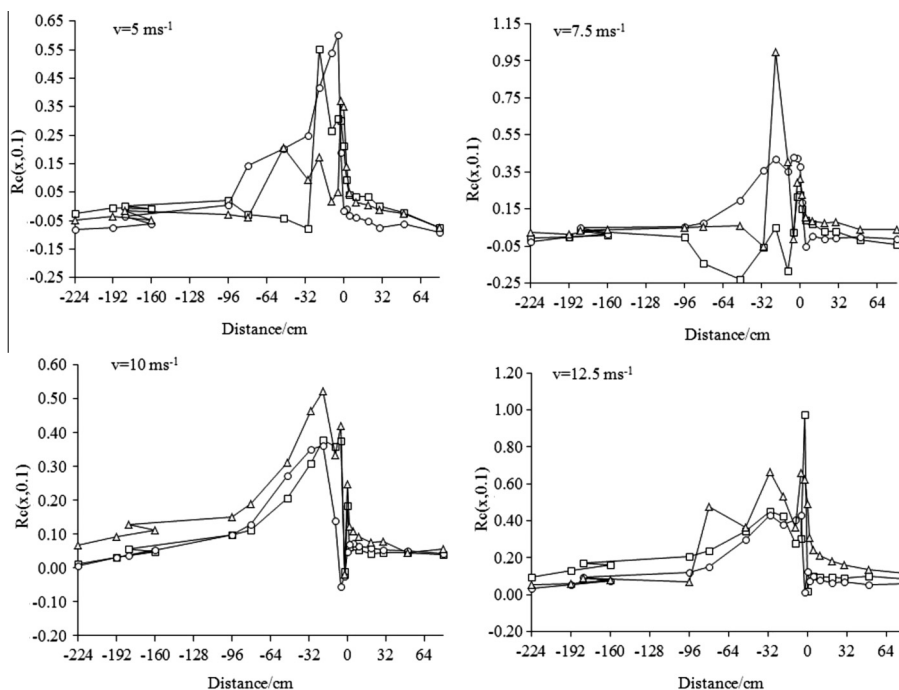
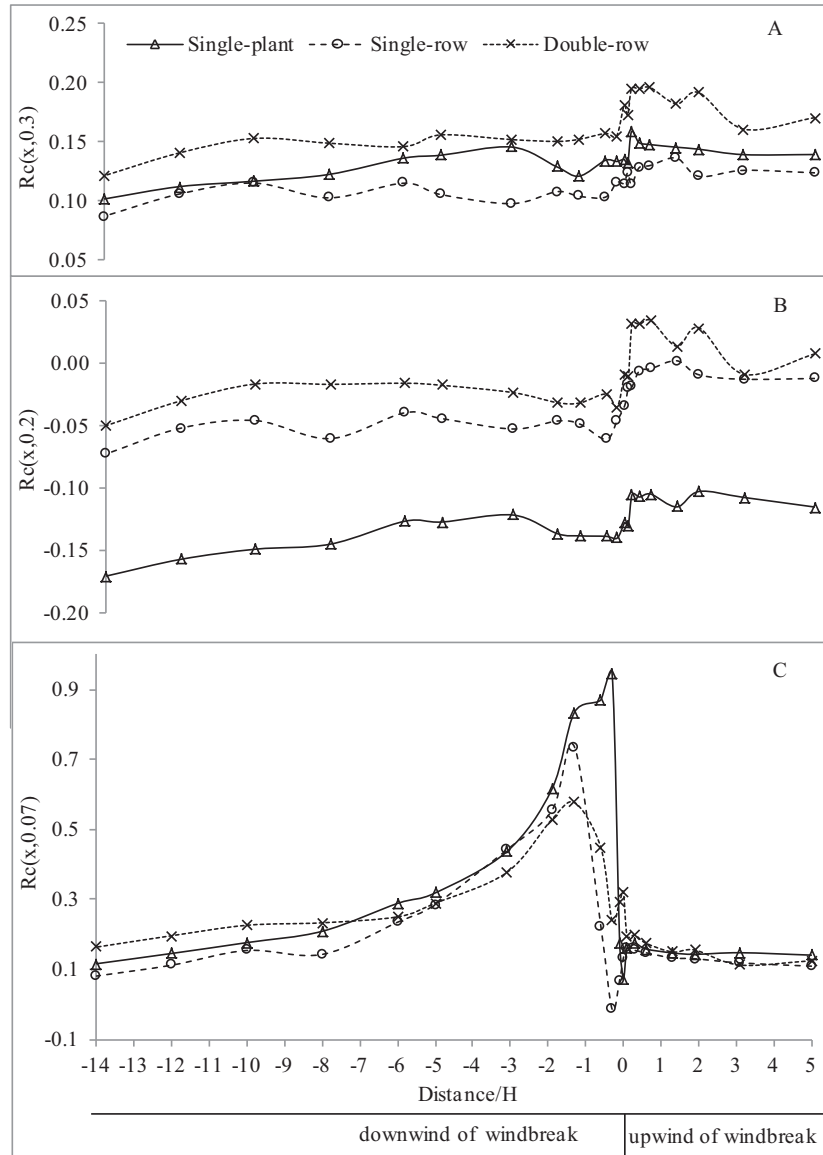


Fig. 6. Reduction coefficient  $R_{c(x, 0.1)}$  for the Artemisia windbreaks at different wind velocities.





**Fig. 7.** Reduction coefficient  $R_{c(x,z)}$  for the Artemisia windbreaks at different heights under a wind velocity of  $10 \text{ m s}^{-1}$  (A) at the height of  $z = 30 \text{ cm}$ ; (B) at the height of  $z = 20 \text{ cm}$ ; (C) at the height of  $z = 7 \text{ cm}$ .

the greatest from upwind  $-0.3 \text{ H}$  to downwind  $-6.0 \text{ H}$  for the single plant Artemisia windbreak. Because the double-row Artemisia windbreak has the highest  $R_{c(x,0.07)}$  from downwind  $-6.0$ , it has the longest shelter distance due to its relatively slower restoration of the wind velocity.

In the area above the windbreak height,  $R_{c(x,0.3)}$  varies, as shown in Fig. 7A. For the double-row Artemisia windbreak,  $R_{c(x,0.3)}$  is the highest upwind, within and downwind of the windbreak, which suggests that the double-row windbreak has the best shelter effect of the Artemisia windbreaks. From these results, we can see that the double-row Artemisia windbreak causes obvious deceleration of the wind velocity in the area above the windbreak height. The magnitude of the acceleration is relatively small in the area at the height of the windbreak. The shelter distance is relatively long in the downwind area below the windbreak height. Therefore, we can conclude that the double-row Artemisia windbreak has the best vertical shelter effect when the wind velocity is  $10 \text{ m s}^{-1}$ .

### 3.2.2. The shelter effect of the Salix windbreaks

#### (1) The horizontal shelter effect

At different wind velocities, the wind velocity reduction coefficient for the Salix windbreaks at a height of  $15 \text{ cm}$  ( $R_{c(x,0.15)}$ ) for each measurement location is shown in Fig. 8.  $R_{c(x,0.15)}$  for each measurement location is generally above zero except within the windbreak, showing that the Salix windbreaks cause an obvious wind velocity reduction. At the lower wind velocity, the  $R_{c(x,0.15)}$  for the measurement locations within both the single plant and single-row Salix windbreaks is at times negative; however, for measurement locations that are within the double-row Salix windbreak, the coefficient is always above zero. This difference in coefficients is caused by the different acceleration zones within the different windbreaks (Fig. 6).  $R_{c(x,0.15)}$  for the measurement locations of the three Salix windbreaks changes with increasing wind velocity. As the wind velocity increases,  $R_{c(x,0.15)}$  for the measurement locations of the double-row Salix windbreak increases, which indicates an increasing shelter effect. When the wind velocity is  $5 \text{ m s}^{-1}$ ,  $R_{c(x,0.15)}$  is greatest upwind for the single plant Salix and greatest downwind for the single-row Salix windbreak, implying that the single-row Salix windbreak has a large shelter effect on the downwind objects. When the wind velocity is  $7.5 \text{ m s}^{-1}$ ,

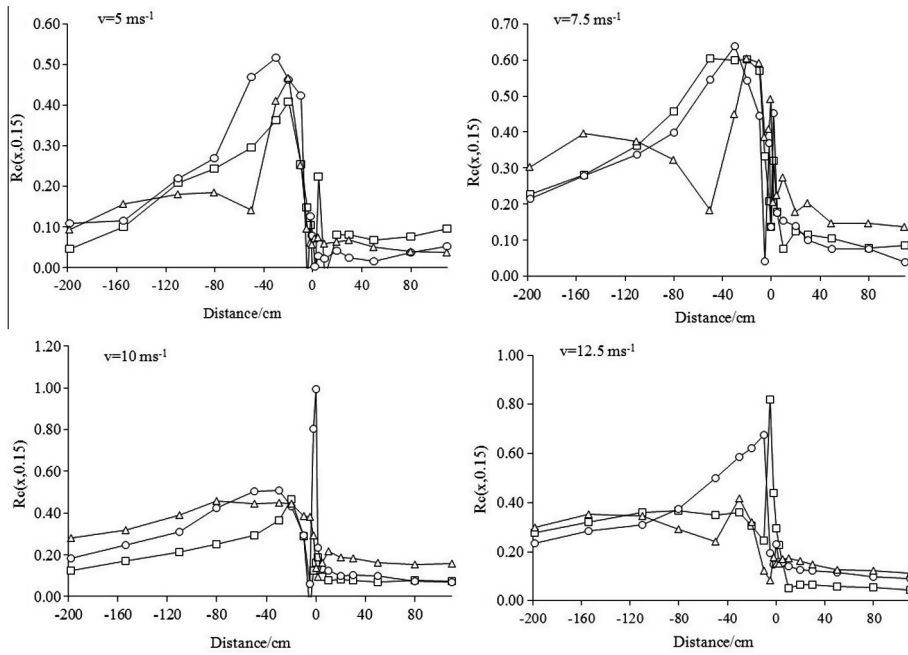


Fig. 8. Reduction coefficient  $R_{c(x,0.15)}$  for the Salix windbreaks at different wind velocities.

$R_{c(x,0.15)}$  for the measurement locations of the double-row Salix windbreak is always the greatest from upwind to downwind  $-0.9$  H except within the windbreak. At that same wind velocity of  $7.5 \text{ m s}^{-1}$ ,  $R_{c(x,0.15)}$  is the greatest from downwind  $-1.4$  H to downwind  $-3.6$  H for the single-row Salix windbreak and is the greatest downwind of  $-3.6$  H for the double-row Salix windbreak. For this wind velocity, we can conclude that the double-row Salix windbreak has the largest shelter effect. When the wind velocity is  $10 \text{ m s}^{-1}$ ,  $R_{c(x,0.15)}$  for the measurement locations of the double-row Salix windbreak is always the greatest upwind of  $0.1$  H and is the greatest within the windbreak for the single-row Salix windbreak, whereas it changes downwind. When the wind velocity is  $12.5 \text{ m s}^{-1}$ ,  $R_{c(x,0.15)}$  for the measurement locations of the double-row Salix windbreak is always the greatest upwind and additionally increases farther downwind of the windbreak. Using these data, we can choose the most appropriate Salix windbreak for the local prevailing wind velocities.

#### (2) The vertical shelter effect

For the Salix windbreaks, when the wind velocity is  $10 \text{ m s}^{-1}$ , the values of  $R_{c(x,z)}$  for the heights of  $7 \text{ cm}$ ,  $20 \text{ cm}$  and  $30 \text{ cm}$  are shown in Fig. 9. The values of  $R_{c(x,z)}$  at a height of  $20 \text{ cm}$  vary as shown in Fig. 9B. For the single plant and single-row Salix windbreaks, the values of  $R_{c(x,z)}$  are all negative, as shown in Fig. 9B, whereas for the double-row Salix windbreaks, the values are all positive. These results are in accordance with the airflow acceleration zones above the three Salix windbreaks in Fig. 5. The magnitude of acceleration is the lowest for the double-row Salix windbreak, with an average  $R_{c(x,z)}$  of  $0.11$ , showing that the wind velocity at this height does not reach the inflow wind velocity. However, this acceleration height does not reach the top of the Salix windbreak ( $H = 22 \text{ cm}$ ). In contrast to the Artemisia windbreaks, the Salix branches are soft enough to bend in the incoming airflow when the wind velocity reaches  $10 \text{ m s}^{-1}$ , which thereby lowers the height of the area of the airflow acceleration.

In the area below the Salix windbreak, at a height of  $7 \text{ cm}$ ,  $R_{c(x,0.07)}$  is the lowest for the double-row Salix windbreaks upwind, within and downwind of the windbreaks (Fig. 9C). Therefore, the double-row Salix windbreak has the largest shelter effect for the areas that are downwind of the windbreak. In the area above the

top of the windbreak,  $R_{c(x,0.3)}$  is the highest from upwind  $5$  H to downwind  $-0.9$  H for the double-row Salix windbreaks, and it is always the lowest from downwind  $-0.9$  H to downwind  $-5$  H for the single-row Salix windbreak (Fig. 9A). The double-row Salix windbreak reduces the wind velocity in the area below the windbreak. Additionally, for the double-row Salix windbreak, the magnitude of acceleration is relatively small for the area at the height that is equal to the windbreak height, and the wind velocity is obviously reduced upwind of the windbreak in the area above the windbreak. Therefore, we can conclude that the double-row Salix windbreak has the largest shelter effect when the wind velocity is  $10 \text{ m s}^{-1}$ .

## 4. Discussion and conclusions

### 4.1. Discussion

We compared the shelter effect of the Artemisia and Salix windbreaks under the same wind velocities. The comparison of the shelter distance of the two windbreaks in the field is shown in Table 2. For the downwind position of approximately  $x = 11 \text{ m}$ , when the wind velocity is  $10 \text{ m s}^{-1}$ ,  $R_{c(x,0.07)}$  is  $0.12$  and  $0.28$ , respectively, for the single plant Artemisia and Salix windbreaks;  $R_{c(x,0.07)}$  is  $0.08$  and  $0.33$ , respectively, for the single-row Artemisia and Salix windbreak; and  $R_{c(x,0.07)}$  is  $0.16$  and  $0.40$ , respectively, for the double-row Artemisia and Salix windbreak. For the single-row windbreaks, the downward shelter distance is approximately  $11.2 \text{ m}$  for the Artemisia windbreak, while it is even longer than  $19.8 \text{ m}$  for the Salix windbreak. Obviously, the Salix windbreaks have a longer shelter distance than the Artemisia windbreaks.

Many previous studies have highlighted the fact that the plant species show differences in their sediment retention capacity, which can be explained by variations in their plant morphological traits (e.g., Burylo et al., 2012b; Erktan and Rey, 2013). Therefore, we also compared the shrubs in our study to those in arid areas in other countries. We found that both Artemisia and Salix show similar features to shrubs in other arid areas of the world. For example, the surveyed Artemisia in our study is on average  $60$ – $130 \text{ cm}$  tall and  $80$ – $170 \text{ cm}$  in diameter; *Aloe secundiflora* and

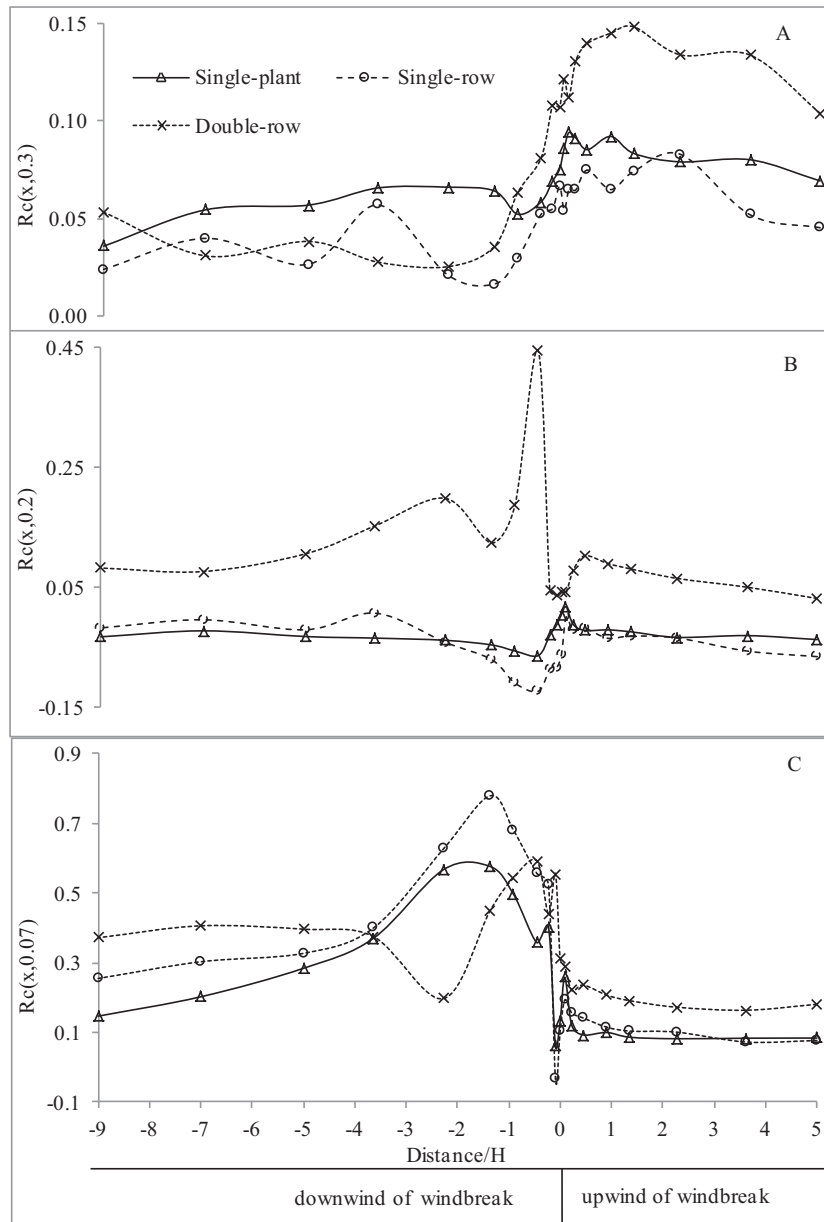


**Fig. 9.** Reduction coefficient  $R_{c(x,z)}$  for the Salix windbreaks at different heights under a wind velocity of  $10 \text{ m s}^{-1}$  (A): at the height of  $z = 30 \text{ cm}$ ; (B): at the height of  $z = 20 \text{ cm}$ ; (C): at the height of  $z = 7 \text{ cm}$ .

*Maerua decumbens* shrubs in Kenya are on average 55–100 cm tall and 70–100 cm in diameter (King, 2008). The surveyed Salix in the study is on average 200–280 cm tall and 150–400 cm in diameter. *Prosopis laevigata* and *Parkinsonia praecox* desert shrubs in Tehuacan, Mexico are on average 260–410 cm tall and 180–410 cm in diameter (Serrano-Vázquez et al., 2013). Therefore, our research results are not limited to only the Mu Us Sandland; they can also be applied to other arid and semi-arid areas.

The shelter effects of a vegetative windbreak can also be influenced by the growth features of the different species of vegetation. Therefore, we also compared the vegetative characteristics of Salix and Artemisia. In sandlands, the annual precipitation is sufficient to meet the growth demands of both Salix and Artemisia in approximately 50% of the years reported (Shi, 2009). Therefore, these two plants can adapt to the local precipitation conditions and can be used as plants for blow-sand control engineering. Vegetation seedling growth characteristics, such as the stem height,

ground coverage and shoot length of both Artemisia and Salix, all increase with increasing precipitation. Increasing precipitation can effectively increase the ground coverage for Artemisia and the stem height as well as the shoot length for Salix. Shi (2009) found that with abundant precipitation (485.3 mm), the ground coverage of Artemisia could reach 90%, thus increasing the efficacy of the vegetation for both checking winds and controlling the movement of near-surface sand. However, when considering the blow-sand control vegetation height, economic value and landscape beautification, Artemisia alone is not ideal for blow-sand control engineering. Given the same precipitation, Salix can produce higher above-ground biomass and incremental stem height than can Artemisia, and thus, Salix can have a longer shelter distance. At the same time, Salix can be used as a raw material for industry, including willow compiling, papermaking and power generation, and thus, it has a higher economic value than Artemisia. Although Salix is an effective blow-sand control plant in terms

**Table 2**  
Shelter distance comparison between *Artemisia* and *Salix* windbreaks.

Distance/m	$R_{c(x,0.07)}$			Distance/m	$R_{c(x,0.07)}$		
	Single plant	Single-row	Double-row		Single plant	Single-row	Double-row
4.00	0.14	0.11	0.13	11.00	0.08	0.08	0.18
2.48	0.15	0.12	0.11	7.92	0.08	0.07	0.16
1.52	0.14	0.13	0.16	5.06	0.08	0.10	0.17
1.04	0.15	0.13	0.15	3.08	0.09	0.10	0.19
0.48	0.16	0.15	0.18	1.98	0.10	0.12	0.21
0.24	0.18	0.15	0.20	1.10	0.09	0.14	0.24
0.08	0.16	0.16	0.20	0.44	0.12	0.16	0.22
0.00	0.07	0.13	0.32	0.22	0.26	0.19	0.29
-0.08	0.18	0.07	0.29	0.00	0.13	0.10	0.31
-0.24	0.95	-0.01	0.24	-0.22	0.06	-0.03	0.55
-0.48	0.87	0.22	0.45	-0.44	0.40	0.52	0.44
-1.04	0.83	0.74	0.58	-1.10	0.36	0.56	0.59
-1.52	0.62	0.55	0.53	-1.98	0.50	0.68	0.54
-2.48	0.44	0.44	0.38	-3.08	0.58	0.78	0.45
-4.00	0.32	0.29	0.29	-5.06	0.57	0.63	0.20
-4.80	0.29	0.24	0.25	-7.92	0.37	0.40	0.37
-6.40	0.21	0.14	0.23	-11.00	0.28	0.33	0.40
-8.00	0.18	0.15	0.23	-15.40	0.20	0.30	0.41
-9.60	0.15	0.11	0.20	-19.80	0.15	0.25	0.37
-11.20	0.12	0.08	0.16				

of the shelter distance, its ground coverage is still usually less than 25%, even under conditions of adequate precipitation (485.3 mm) (Shi, 2009). Blowing sand tends to be more active near the surface. This finding suggests that planting only *Salix* will not effectively control the sand storms.

Considering the vegetative characteristics and blow-sand control features of the *Salix* and *Artemisia* windbreaks, it is optimal to plant these two windbreaks together in a system for blow-sand control engineering. In this blow-sand control system, the *Salix* windbreaks are planted as a shelter forest, and the *Artemisia* windbreaks are planted as near-surface barriers. The system not only can integrate blow-sand control and landscape beautification but also can produce economic value for the local people of the sandland. Although the optimal design depends strongly on the purpose for which it is constructed, such as the protection of a field from erosion or the protection of infrastructure from being buried (Cornelis and Gabriels, 2005), it is also important to understand the general abilities of the windbreaks in reducing the wind velocity. Therefore, our study results are useful both for the construction of windbreaks in the Mu Us Sandland and for insight into blow-sand control engineering throughout semi-arid China.

#### 4.2. Conclusions

Based on a field survey of sand-dust sources in the Mu Us Sandland, we simulated the airflow around vegetative windbreaks in a wind tunnel and analyzed their shelter effects. For the single plant *Artemisia* windbreak, as the inflow wind velocity increases, the wind velocity increases more around the two side areas of the plant, with low values in the leeward areas. Seven new velocity zones in the horizontal direction, including four deceleration zones and three acceleration zones, are formed when airflow passes through the *Artemisia* windbreaks. When we increase the number of clusters and the number of rows of trees in the windbreaks, the number of velocity zones does not change; however, the airflow restoration velocity decreases, the scale of the vortex zone decreases, and the shelter distance becomes longer.

The velocity isolines around the single plant *Salix* windbreak are sparser compared with those around the single plant *Artemisia* windbreaks due to the difference in the two plants' shape characteristics. The mean velocity field in the horizontal direction that is affected by the *Salix* windbreaks could be divided into the airflow

deceleration zone before the windbreak, the airflow acceleration zone above the windbreak, the vortex zone behind the windbreak and the downwind airflow restoration zone. The area of deceleration in front of the double-row *Salix* windbreak is larger than that of either the single plant or the single-row *Salix* windbreak. The magnitude of the wind velocity reduction for the double-row *Salix* windbreak is also much greater than that of the other windbreaks. When the airflow accelerates as it passes over the *Salix* windbreaks, the airflow direction experiences a transition from upwind to horizontal to downwind. In this acceleration zone, the double-row *Salix* windbreak has a weak acceleration effect. In addition, the restoration of the wind velocity is relatively slow because only a minimal vortex zone exists leeward of the double-row *Salix* windbreak. Therefore, the downwind area of the wind velocity restoration is larger than that of the other two *Salix* windbreaks; in addition, the double-row *Salix* windbreak has a longer shelter distance than the others.

Our research indicates that with increasing wind velocity, the more complexly constructed *Artemisia* windbreaks have a larger shelter effect than the more simply constructed windbreaks. The *Salix* windbreaks show trends that are similar to those of the *Artemisia* windbreaks. However, under a similar wind velocity, *Salix* windbreaks have a longer shelter distance than *Artemisia* windbreaks because *Salix* is higher than *Artemisia*. Both *Artemisia* and *Salix* are mainly distributed as single plants in natural sandlands, while we usually plant single-row or multi-row vegetative windbreaks in sand-blown engineering. Therefore, we need to ascertain which windbreak has a better shelter effect in sand-control engineering.

#### Acknowledgments

This work was financially supported by the National Natural Science Foundation of China (Grants No. 41101002 and No. 41330746), the Fundamental Research Funds for the Central Universities (2013YB46). The authors greatly appreciate the assistance of M.Sc. Niu Yanping from Heibei Normal University with the wind tunnel experiment, Dr. Gao Han from Beijing Forestry University with model-making in the wind tunnel test, M.Sc. Qian Jiang and Dr. Wang Rende from Beijing Normal University for help in field measurements, and Elsevier's English Language Editing Webshop for language editing.

## References

- Banzhaf, J., Leihner, D.E., Buerkert, A., Serafini, P.G., 1992. Soil tillage and wind break effects on millet and cowpea: I. Wind speed, evaporation, and wind erosion. *Agron. J.* 84, 1056–1060.
- Burylo, M., Hudek, C., Rey, F., 2011. Soil reinforcement by the roots of six dominant species on eroded mountainous marly slopes (Southern Alps, France). *Catena* 84 (1–2), 70–78.
- Burylo, M., Rey, F., Mathys, N., Dutoit, T., 2012a. Plant root traits affecting the resistance of soils to concentrated flow erosion. *Earth Surf. Proc. Land.* 37 (14), 1463–1470.
- Burylo, M., Rey, F., Bochet, E., Dutoit, T., 2012b. Plant functional traits and species ability for sediment retention during concentrated flow erosion. *Plant Soil* 353 (1–2), 135–144.
- Chepil, W.S., Woodruff, N.P., 1963. The physics of wind erosion and its control. *Adv. Agron.* 15, 211–302.
- Cornelis, W.M., Gabriels, D., 2005. Optimal windbreak design for wind-erosion control. *J. Arid Environ.* 61 (2), 315–332.
- Decai, Z., 1998. *Dynamical Evolution of Sand Sea in China*. Gansu Culture Press, p. 20.
- Dong, Z., Li, H.L., Wang, J., Ding, G.D., Sun, B.P., 2007. Wind tunnel test on effect of controlling wind and deposited sand of geogrid sand-barrier. *Sci. Soil Water Conserv.* 5 (1), 35–39 (in Chinese).
- Dregan, H.E., 1998. Desertification assessment. In: Lal, R., Blum, W.H., Valentine, C., Stewart, B.A. (Eds.), *Method of Assessment for Soil Degradation*. CRC Press, New York, pp. 441–458.
- Erktan, A., Rey, F., 2013. Linking sediment trapping efficiency with morphological traits of *Salix* tiller barriers on marly gully floors under ecological rehabilitation. *Ecol. Eng.* 51, 212–220.
- FAO. 1978. *Soil erosion by Wind and Measures for its control (fourth ed.)*. FAO Agricultural Development Paper. 71, Rome.
- García-Estringana, P., Alonso-Blázquez, N., Marques, M.J., Bienes, R., González-Andrés, F., Alegre, J., 2013. Use of Mediterranean legume shrubs to control soil erosion and runoff in central Spain. A large-plot assessment under natural rainfall conducted during the stages of shrub establishment and subsequent colonization. *Catena* 102, 3–12.
- González-Ruiz, T., Rodríguez-Zaragoza, S., Ferrera-Cerrato, R., 2007. Fertility islands around *Prosopis laevigata* and *Pachycereus hollianus* in the dry lands of Zapotitlan Salinas, Mexico. *J. Arid Environ.* 72, 1202–1212.
- Hagen, L.J., Skidmore, E.L., 1971. Windbreak drag as influenced by porosity. *Trans. ASAE* 9, 74–76.
- He, D.X., Chen, K., Zhang, L.L., 2006. *Wind Engineering and Industrial Aerodynamics*. National Defense Industry Press, Beijing, p. 18, (in Chinese).
- Judd, M.J., Raupach, M.R., Finnigan, J.J., 1996. A wind tunnel study of turbulent flow around single and multiple windbreaks. Part I: velocity fields. *Boundary Layer Meteorol.* 80, 127–165.
- King, E.G., 2008. Facilitative effects of *Aloe secundiflora* shrubs in degraded semi-arid rangelands in Kenya. *J. Arid Environ.* 72, 358–369.
- Li, B., 1990. *A Survey on the Natural Resources and Environment on Ordos Plateau in Inner Mongolia*. Science Press, Beijing, pp. 72–125, p. 225 (in Chinese).
- Li, G.S., Qu, J.J., Han, Q.J., Fang, H.Y., Wang, W.F., 2013. Responses of three typical plants to wind erosion in the shrub belts atop Mogao Grottoes, China. *Ecol. Eng.* 57, 293–296.
- Perera, M.D.A.E.S., 1981. Shelter behind two-dimensional solid and porous fences. *J. Wind Eng. Ind. Aerodyn.* 8, 93–104.
- Perroni-Ventura, Y., Montaña, C., García-Oliva, F., 2006. Relationship between soil nutrient availability and plant species richness in a tropical semiarid environment. *J. Veg. Sci.* 17 (6), 719–728.
- Qu, J.J., Liu, X.W., Lei, J.Q., Li, F., Yu, Z.Y., 2001. Simulation experiments on sand-arresting effect of nylon net fence in wind tunnel. *J. Desert Res.* 21, 276–280 (in Chinese).
- Rosenberg, N.J., 1974. *Microclimate: The Biological Environment*. Wiley, New York.
- Serrano-Vázquez, A., Rodríguez-Zaragoza, S., Pérez-Juárez, H., Bazán-Cuenca, J., Rivera-Aguilar, V.M., Durán, A., 2013. Physical and chemical variations of the soil under two desert shrubs in Tehuacan, Mexico. *Soil Sci.* 178, 87–103.
- Shi, S., 2009. *Vegetation Restoration/Reestablishment for Protection a Town in Semiarid Region from Blown-sand Disaster—A case study on Dabqig of Uxin Qi*. Beijing Normal University, China (in Chinese).
- Wu, B., Yang, H., 2013. Spatial patterns and natural recruitment of native shrubs in a semi-arid sandy land. *PLoS ONE* 8 (3), e58331. <http://dx.doi.org/10.1371/journal.pone.0058331>.
- Wu, X.X., Zou, X.Y., 2011. Research on characteristic and density of sand-blown activity in Uxin Qi. *J. Nat. Disasters* 20 (1), 134–141 (in Chinese).
- Wu, Z., 2003. *Geomorphology of Wind-drift Sands and their Controlled Engineering*. Science Press, Beijing, pp. 332–403 (in Chinese).
- Wu, X.X., Zou, X.Y., Zheng, C.Z.Q., Zhang, C.L., 2011. Field measurement and wind-tunnel simulation of airflow field over the stoss slope on barchan dune. *J. Arid Environ.* 75, 438–445.
- Wu, X.X., Zou, X.Y., Zhang, C.L., Wang, R.D., Zhao, J.Y., Zhang, J.Q., 2013. The effect of wind barriers on airflow in a wind tunnel. *J. Arid Environ.* 97, 73–83.
- Yang, H., Lu, Q., Wu, B., Yang, H., Zhang, J., et al., 2006. Vegetation diversity and its application in sandy desert revegetation on Tibetan Plateau. *J. Arid Environ.* 65, 619–631.
- Zhang, X., 1994. The ecological background of the Mu Us sandland and the principles and optimal models for grassland management. *Acta Phytocol. Sin.* 18, 1–16 (in Chinese with English abstract).
- Zhang, X.S., Shi, P.J., 2003. Theory and practice of marginal ecosystem management: establishment of optimized eco-productive paradigm of grassland and farming-pastoral zone of northern China. *Acta Bot. Sin.* 45, 1135–1138.
- Zhang, Y., Cao, C.Y., Han, X.S., Jiang, S.Y., 2013. Soil nutrient and microbiological property recoveries via native shrub and semi-shrub plantations on moving sand dunes in Northeast China. *Ecol. Eng.* 53, 1–5.
- Zhao, H.L., Masayuki, A., 1997. Study on desertification mechanism of grazing grassland in Kerqin sandy land in inner Mongolia, China. *Grassland China* 3, 15–23.
- Zhong, D.C., Qu, J.J., 2003. Recent development trend and prediction of sand deserts in China. *J. Arid Environ.* 53, 317–329.
- Zhu, Z.D., Cheng, G.T., 1994. *China Land Desertification*. Science Press, Beijing, 1–2.